Embedded Near-Field Probing Antenna for Enhancing the Performance of 37–41-GHz Linear and Dual-Polarized Phased Antenna Arrays

Huixin Jin, *Student Member, IEEE*, Ahmed Ben Ayed, *Graduate Student Member, IEEE*, Ziran He, *Member, IEEE*, Bernard Tung, *Graduate Student Member, IEEE*, and Slim Boumaiza, *Senior Member, IEEE*

***Abstract*— This letter proposes a new wideband near-field (NF) probing antenna embedded in millimeter-phased antenna arrays to produce the feedback signals necessary for carrying-out array calibration and digital pre-distortion (DPD) training. Specifically, the topology and layout of the proposed NF probing antenna are carefully devised to avoid disturbing the antenna array's radiation pattern while providing a coupling to its surrounding antenna elements with flat magnitude and constant group delay in both vertical and horizontal polarizations. Moreover, the proposed NF probing antenna size is optimized to cope with the constrained spacing between the antenna elements (e.g., $\lambda/2$ antenna spacing). Proof-of-concept prototypes of a 2 × 2 dual-polarized passive and a 4 × 4 linear-polarized active antenna arrays with embedded NF probing antenna(s) operating over the frequency band of 37–41 GHz were designed. Moreover, a 4 × 4 linear-polarized antenna array without NF probing antennas was also fabricated to serve as a benchmark. The measurement confirmed the negligible impact of the NF probing antennas on the antenna array's radiation pattern. Furthermore, the embedded NF probing antennas were successfully used to train a DPD function which then enabled the effective isotropic radiated power to be increased from 32 to 34.1 dBm while maintaining an error vector magnitude (EVM) below 3.5%.**

***Index Terms*— Beamforming antenna arrays, calibration, digital pre-distortion (DPD), dual-polarization, millimeter-wave (mm-wave), near-field (NF), phased arrays.**

I. Introduction

MILLIMETER-WAVE (mm-wave) antenna arrays will play an important role in future wireless communication systems. These arrays are commonly implemented using multiple power amplifiers (PAs) following a radio frequency (RF) beamforming architecture and have built-in phase and magnitude control components. Errors in the phase and amplitude control circuitry of these arrays can result in radiation pattern distortions and degrade the link-level performance metrics. Moreover, these arrays exhibit non-negligible non-linearities when operated in their efficient region. The deployment of calibration and digital pre-distortion (DPD) training methods for in-field antenna array performance enhancement is, hence, critical for the successful deployment of these arrays.

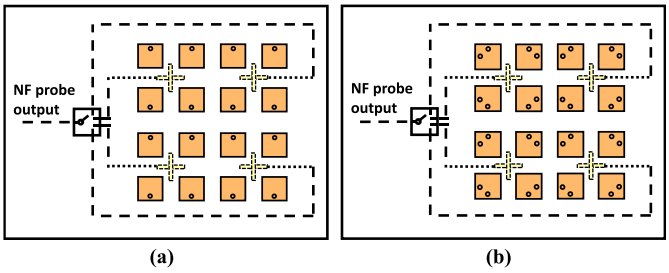

Fig. 1. Block diagram of a linear and dual-polarized RF beamforming antenna arrays with proposed embedded NF probing antennas.

Different techniques have been proposed in the literature for antenna array calibration and DPD training. Chae et al. [1] and Tervo et al. [2] proposed a coupler-based feedback method where the couplers are laid out to have a single output while coupling to the different PAs outputs in the array. Implementing couplers at the PA outputs, however, imposed larger antenna spacing which consequently reduces the array steering range. Alternatively, Brautigam et al. [3], Aoki et al. [4], Ng et al. [5], Dey et al. [6], and Löhning et al. [7] proposed over-the-air (OTA) based feedback methods for array calibration and DPD training, where a far-field (FF) probe was used in [3], [4], and [5], and probes placed in the near-field (NF) region of the phased array were used in [6] and [7]. While these methods can enhance the performance of mm-wave RF beamforming antenna arrays, the use of OTA-based feedback methods, in practice, poses challenges at the deployment stage. Conversely, the concept of NF probing antennas embedded within the phased array has emerged as a promising method to observe the transmitter and improve its performance while eliminating the need for challenging OTA probes or couplers at the PA outputs. In addition, Shipley and Woods [8] exploited the mutual coupling between the antenna elements to calibrate the antenna array. This approach, however, requires dedicated analog converters per antenna chain, hence it is not suitable for RF beamforming antenna arrays. Ayed et al. [9] and Cao et al. [10] used an array of NF probe(s) embedded within the antenna array to serve as feedback for self-calibration. However, the

Manuscript received 24 February 2023; revised 12 April 2023; accepted 15 April 2023. This work was supported in part by the Ontario Research Funds-Research Excellence and in part by the Natural Sciences and Engineering Research Council of Canada (NSERC). *(Corresponding author: Huixin Jin.)*

The authors are with the Department of Electrical and Computer Engineering, University of Waterloo, Waterloo, ON N2L 3G1, Canada (e-mail: huixin.jin@uwaterloo.ca).

This article was presented at the IEEE MTT-S International Microwave Symposium (IMS 2023), San Diego, CA, USA, June 11–16, 2023.

Color versions of one or more figures in this letter are available at https://doi.org/10.1109/LMWT.2023.3268570.

Digital Object Identifier 10.1109/LMWT.2023.3268570

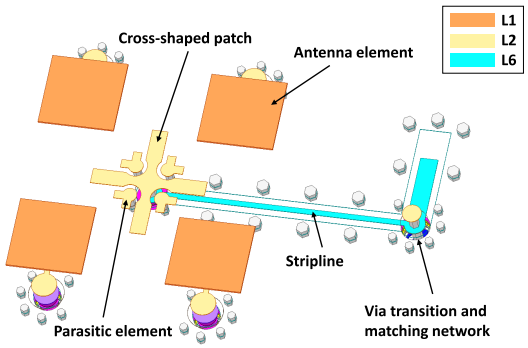

Fig. 2. Layout of the proposed NF probing antenna design embedded within a 2 × 2 antenna array.

NF probes used in [10] are not compatible with dual-polarized antenna arrays.

In this work, a novel wideband NF probing antenna design that is suitable for enhancing the performance of linear and dual-polarized RF beamforming antenna arrays operating in the 37–4-GHz frequency band is proposed. Specifically, the topology and layout of the proposed NF probing antenna are carefully devised to avoid disturbing the antenna array's radiation patterns, while also providing flat coupling magnitude and constant group delay to its surrounding elements in both vertical and horizontal polarizations. The flat coupling magnitude and constant group delay between the NF probing antennas and the radiating ones are key requirements to enable the use of NF probing antennas for accurate array calibration and DPD training. Moreover, the proposed NF probing antenna design has a low profile and is scalable to larger antenna arrays. Proof-of-concept prototypes of a 2 × 2 dual-polarized passive and a 4 × 4 linear-polarized active antenna arrays with embedded NF probing antennas are presented. Moreover, the application of these NF probing antennas to DPD training is demonstrated.

II. Proposed NF Probing Antenna Design

In this section, the design consideration and layout of the proposed NF probing antenna for enhancing the performance of linear and dual-polarized antenna arrays are presented, where the conceptual diagrams of 4 × 4 linear and dual-polarized antenna arrays with proposed embedded NF probing antennas are shown in Fig. 1(a) and (b), respectively. Fig. 2 shows the layout of the proposed NF probing antenna design within a 2 × 2 antenna array with antenna spacing of $\lambda/2$ at 38.5 GHz. The NF probing antenna has a symmetrical cross-shaped patch with coaxial feeding which is designed to obtain flat magnitude and constant group delay coupling behavior to its surrounding antenna elements in both vertical and horizontal polarizations over 37–41-GHz frequency band. In addition, the four parasitic elements are also designed symmetrically toward the center of the NF probe for better input matching and coupling flatness. Moreover, the size of the NF probing antenna was optimized to fit within a constrained antenna spacing without affecting its radiation pattern.

To validate the performance of the proposed NF probing antenna within an antenna array, a 2 × 2 and a 4 × 4 antenna array prototypes were simulated, and later fabricated, using the stack-up shown in Fig. 3. The substrate used in this design is Isola ASTRA MT77 characterized by a dielectric constant of 3 and loss tangent of 0.0017. The antenna elements of the proposed array prototypes use a proximity-coupled feed

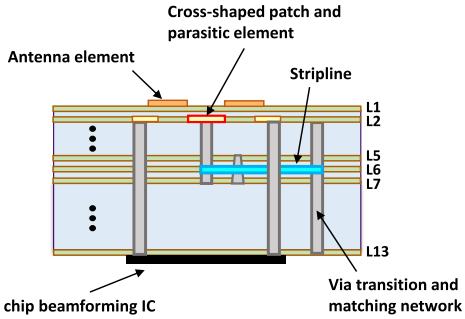

Fig. 3. Stack-up of the designed antenna array with the proposed NF probing antennas embedded.

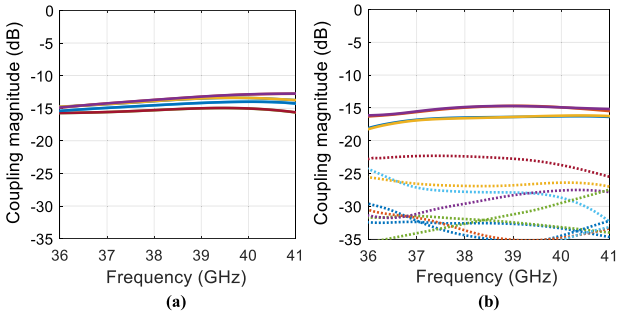

Fig. 4. Simulation results of NF probing antenna embedded in (a) 2 × 2 passive dual-polarized antenna array and (b) 4 × 4 active linear-polarized antenna array. The solid curves represent the coupling magnitudes between the embedded NF probe and the four closest antenna elements, while dotted lines are the coupling magnitudes between the embedded NF probe and the further 12 antenna elements.

structure, where the antenna patch is located on L1 and its microstrip feed line is on L2, with L5 being the antenna ground. The RF beamforming ICs are placed on L13, while L7–L12 are used for power planes, digital signal routings, and RF grounds. Proximity feed is selected in this design based on optimizing antenna bandwidth and beamforming IC routing constraints. The microstrip feed line on L2 is connected to the bottom layer (L13) through an L2–L13 mechanical via. L2 layer is also used to house the proposed NF probing antenna. The latter cannot be routed directly to L13 using an L2–L13 mechanical via transition as it is directly above the IC footprint. Moreover, performing any routing on L2 would break the symmetry in the NF probe antenna structure and impact its performance. To alleviate this issue, the NF probing antenna is routed to L13 through an L2–L7 mechanical via, a stripline on L6, and an L2–L13 mechanical via. Note, the use of the L2–L7 via to transition from L2 to L6 and the use of the L2–L13 via to transition between L6 and L13 result in non-avoidable stubs in the transitions that must be taken into account during the design process. This was necessary to maximize the tradeoff between the different via types, the number of lamination cycles, and the complexity of the printed circuit board (PCB) stack-up.

Fig. 4(a) and (b) depict the results of the electromagnetic (EM) simulation of 2 × 2 dual-polarized and 4 × 4 linear-polarized arrays with the embedded NF probing antenna, respectively. The solid lines in Fig. 4(a) and (b) represent the coupling magnitudes between the embedded NF probe and the four closest antenna elements, while the dotted lines in Fig. 4(b) depict the coupling magnitudes between the embedded NF probe and the remaining antenna elements of the 4 × 4 array. The spacing between the antenna elements is 3.9 mm which is $\lambda/2$ at 38.5 GHz. Fig. 4(a) and (b) shows a variation in the coupling factor's magnitude, and group delay

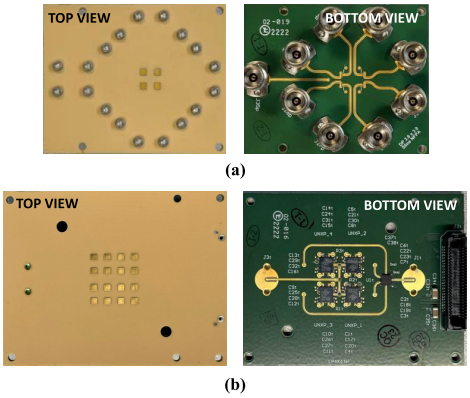

Fig. 5. Photographs of fabricated (a) 2 × 2 dual-polarized passive antenna array and (b) 4 × 4 linear-polarized active antenna array.

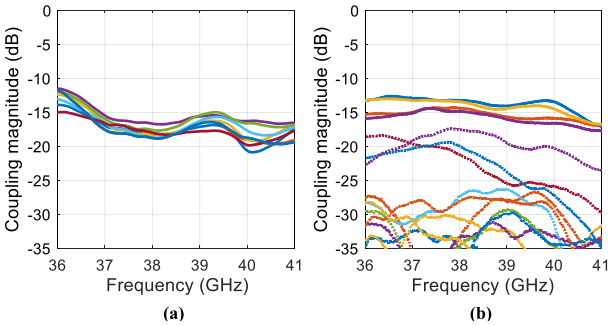

Fig. 6. Measured magnitude of the coupling between an NF probing antenna and the radiating antenna elements when the NF probing antenna is integrated into (a) 2 × 2 dual-polarized array and (b) 4 × 4 linear-polarized array.

of less than 3 dB and 140 ps, respectively, from 36 to 41 GHz. Furthermore, when a radiating element is fed with a modulated signal having an 800 MHz modulation bandwidth and a carrier frequency of 38.5 GHz, the NF probing antenna output signal exhibited a normalized root-mean-square error (NRMSE) and error vector magnitude (EVM) of less than 1.6% and 0.025%, respectively, for both antenna arrays.

III. Validation Results

In this section, the performance of the proposed NF probing antenna on the fabricated proof-of-concept 2 × 2 dual-polarized passive and 4 × 4 linear-polarized active antenna array prototypes shown in Fig. 5 is assessed. Note, in the fabricated 4 × 4 active antenna array, the outputs of the embedded NF probing antennas are routed on the bottom layer using a co-planar waveguide ground line to a single-pole four-throw (SP4T) switch for system-level testing simplicity. In order to assess the impact of the NF probing antennas on the radiation pattern of the fabricated 4 × 4 antenna array, a 4 × 4 linear-polarized active antenna array without NF probing antennas was also fabricated using the same antenna structure and PCB stack-up to serve as a benchmark. The continuous-wave (CW) measurements presented in this section were conducted using a vector network analyzer (VNA). The array under test (AUT) was mounted on a servo motor. A horn antenna was used to capture the FF signal. The output of the horn antenna and the NF probes were fed back to the VNA to be captured. Moreover, the vector-modulated test signal used in the experiment was generated using a 12-bit, 12 GS/s arbitrary waveform generator (M8190A from Keysight Technologies), with output centered at an intermediate frequency of 2 GHz. An IQ-mixer (ADMV-1013) was used to up-convert the IF signal to a center frequency

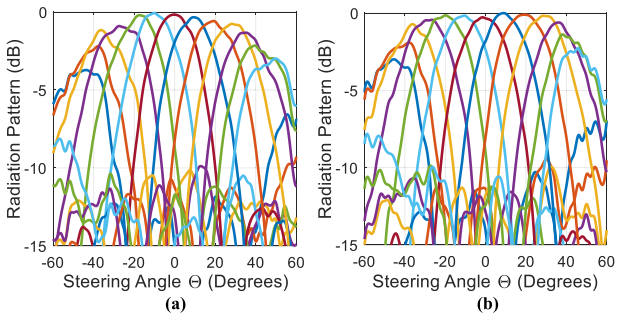

Fig. 7. Measured radiation patterns versus different steering angles for (a) fabricated reference array without NF probes and (b) fabricated array with the proposed embedded NF probes.

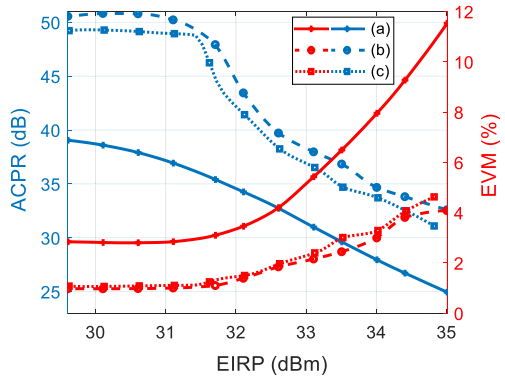

Fig. 8. Measured ACPR and EVM at the FF probe versus EIRP when the 4 × 4 antenna array is fed with a 400 MHz OFDM signal. (a) Prior to DPD. (b) After DPD trained at the FF in the main beam direction. (c) After DPD trained using NF probing antennas.

of 37.5 GHz. The signal was then amplified using a driver amplifier and fed to the AUT when performing the modulated measurements. A local oscillator source (MXG-N5183B from Keysight Technologies) was used to drive the up-conversion board used in the setup. Note, the array calibration was performed with the AUT input connected to the VNA.

Fig. 6(a) and (b) shows the measured coupling magnitudes between the proposed NF probing antenna and the array antenna elements: (a) in the 2 × 2 dual-polarized passive antenna array and (b) in the 4 × 4 linear-polarized antenna array. From Fig. 6(a), it is clear that the proposed NF probing antenna can achieve flat coupling response in both horizontal and vertical polarizations where the coupling magnitude varied by less than 7 dB from 37 to 41 GHz. In Fig. 6(b), four NF probing antennas are integrated into a 4 × 4 linear-polarized array, and the measured results showed a variation of less than 4 dB in coupling magnitude across the designed bandwidth. In terms of the group delay, the variation is less than 240 ps in the 2 × 2 case and 85 ps in the 4 × 4 case. Note, the results in Fig. 6(a) and (b) show good agreement with the corresponding simulation results in Fig. 4, with some discrepancies attributed to PCB fabrication errors. The measured radiation pattern of the 4 × 4 linear-polarized array without NF probes as shown in Fig. 7(a), and with the proposed NF probing antennas embedded as shown in Fig. 7(b) when both arrays are steered between ±50°. From Fig. 7(a) and (b), it is clear that the array radiation pattern was not affected when the proposed NF probing antenna is included in the antenna array.

In order to demonstrate the applicability of NF probing antennas to enhance the performance of mm-wave beamforming antenna arrays, the array was driven with a 256-QAM 400 MHz OFDM signal, and the NF probe output signals

were used to train a DPD function and linearize the array following the procedure described in [11]. Fig. 8 shows the adjacent channel power ratio (ACPR) and EVM results at the FF probe versus the EIRP: (a) prior to DPD, (b) after DPD trained at the FF in the main beam direction, and (c) after DPD trained using the outputs of NF probing antennas [11]. From Fig. 8, it is evident that the DPD trained using the NF probing antennas in (c) achieves similar results to the DPD trained at the FF (b). For instance, when the EIRP is set to 34 dBm, the ACPR and EVM improved from 27 dB and 8.3% before DPD, to 34.4 dB and 3.2% in (b), and 33.4 dB and 3.4% in (c), respectively. Note, using DPD trained with the NF probing antennas as feedback, the EIRP is increased by 2 dB from 32.11 to 33.4 dBm while meeting or exceeding the 3GPP EVM and ACPR standard of 3.5% and 26 dB requirement.

IV. Conclusion

In this letter, a wideband NF probing antenna suitable for enhancing the performance of linear and dual-polarized RF beamforming antenna arrays operating in 37-41-GHz frequency band was proposed. Simulation and measurement results on proof-of-concept prototypes of a 2×2 dual-polarized passive and a 4×4 linear-polarized active antenna arrays with embedded NF probing antenna confirmed the capacity of the proposed NF probing antenna maintained a coupling to its surrounding elements with flat magnitude and constant group delay in both array polarizations, i.e., vertical and horizontal polarizations, with negligible impact of the antenna array's radiation pattern with NF probing antennas embedded. Furthermore, the embedded NF probing antennas in the 4×4 linear-polarized active array prototype were successfully used to train a DPD function which then enabled the effective isotropic radiated power to be increased from 32 to 34.1 dBm while maintaining an EVM below 3.5%.

Acknowledgment

The authors would like to acknowledge Gorilla Circuits for array fabrication, and NXP Semiconductors for supplying the integrated circuits used in the fabricated active arrays.

References

[1] S.-C. Chae, H.-W. Jo, J.-I. Oh, G. Kim, and J.-W. Yu, "Coupler integrated microstrip patch linear phased array for self-calibration," *IEEE Antennas Wireless Propag. Lett.*, vol. 19, no. 9, pp. 1615–1619, Sep. 2020.

[2] N. Tervo et al., "Digital predistortion of millimeter-wave phased array transmitter with over-the-air calibrated simplified conductive feedback architecture," in *IEEE MTT-S Int. Microw. Symp. Dig.*, Aug. 2020, pp. 543–546.

[3] B. Bräutigam, M. Schwerdt, M. Bachmann, and M. Stangl, "Individual T/R module characterisation of the Terrasar-X active phased array antenna by calibration pulse sequences with orthogonal codes," in *Proc. IEEE Int. Geosci. Remote Sens. Symp.*, Barcelona, Spain, Jul. 2007, pp. 5202–5205.

[4] Y. Aoki et al., "An intermodulation distortion oriented 256-element phased-array calibration for 5G base station," in *IEEE MTT-S Int. Microw. Symp. Dig.*, Denver, CO, USA, Feb. 2022, pp. 518–521.

[5] E. Ng, Y. Beltagy, G. Scarlato, A. B. Ayed, P. Mitran, and S. Boumaiza, "Digital predistortion of millimeter-wave RF beamforming arrays using low number of steering angle-dependent coefficient sets," in *Proc. IEEE Trans. Microw. Theory Tech.*, Jul. 2019, pp. 481–484.

[6] U. Dey, J. Hesselbarth, J. Moreira, and K. Dabrowiecki, "Over-the-air test of dipole and patch antenna arrays at 28 GHz by probing them in the reactive near-field," in *Proc. 95th ARFTG Microw. Meas. Conf. (ARFTG)*, Aug. 2020, pp. 1–4.

[7] M. Lohning, T. Deckert, V. Kotzsch, and M. V. Bossche, "A novel OTA near-field measurement approach suitable for 5G mmWave wideband modulated tests," in *IEEE MTT-S Int. Microw. Symp. Dig.*, Jun. 2022, pp. 856–858.

[8] C. Shipley and D. Woods, "Mutual coupling-based calibration of phased array antennas," in *Proc. IEEE Int. Conf. Phased Array Syst. Technol.*, May 2000, pp. 529–532.

[9] A. B. Ayed, G. Scarlato, P. Mitran, and S. Boumaiza, "On the effectiveness of near-field feedback for digital pre-distortion of millimeter-wave RF beamforming arrays," in *IEEE MTT-S Int. Microw. Symp. Dig.*, Aug. 2020, pp. 547–550.

[10] Y. Cao, A. B. Ayed, J. Xia, and S. Boumaiza, "Uniformly distributed near-field probing array for enhancing the performance of 5G millimeter-wave beamforming transmitters," *IEEE Microw. Wireless Compon. Lett.*, vol. 31, no. 6, pp. 823–826, Jun. 2021.

[11] A. B. Ayed, Y. Cao, P. Mitran, and S. Boumaiza, "Digital predistortion of millimeter-wave arrays using near-field based transmitter observation receivers," *IEEE Trans. Microw. Theory Techn.*, vol. 70, no. 7, pp. 3713–3723, Jul. 2022.